References

CROMER, D. T. & MANN, J. B. (1968). *Acta Cryst.* A**24**, 321–324.
HALL, S. R. & STEWART, J. M. (1973). *Can. Mineral.* **12**, 169–177.
JAMES, R. W. (1967). *The Optical Principles of the Diffraction of X-rays.* London: Bell.
KNOP, O., HUANG, C. & WOODHAMS, F. W. D. (1970). *Am. Mineral.* **55**, 1115–1130.
KNOP, O., IBARAHIM, M. A. & SUTARNO (1965). *Can. Mineral.* **8**, 291–324.
LINDQVIST, M., LUNDQVIST, D. & WESTGREN, A. (1936). *Sven. Kem. Tidskr.* **48**, 156–160.
NAKAZAWA, H., TSUKIMURA, K., HIRAI, H. & WADA, H. (1983). *Acta Cryst.* B**39**, 532–535.
RAJAMANI, V. & PREWITT, C. T. (1973). *Can. Mineral.* **12**, 178–187.
RAJAMANI, V. & PREWITT, C. T. (1975). *Am. Mineral.* **60**, 39–48.
RIECK, G. D. & DRIESSENS, F. C. M. (1966). *Acta Cryst.* **20**, 521–525.
SKOLNICK, L. P., KONDO, S. & LAVINE, L. R. (1958). *J. Appl. Phys.* **29**, 198–203.
VAUGHAN, D. J. & RIDOUT, M. S. (1971). *J. Inorg. Nucl. Chem.* **33**, 741–746.
YAKEL, H. L. (1980). *J. Phys. Chem. Solids*, **41**, 1097–1104.
YAKEL, H. L. (1983). *Acta Cryst.* B**39**, 20–28.
YAMANAKA, T. & NAKAHIRA, M. (1973). *Mineral. J.* **7**, 202–220.

Acta Cryst. (1984). B**40**, 367–372.

Time-of-Flight Neutron Diffraction Study of a Single Crystal of Yttria-Stabilized Zirconia, $Zr(Y)O_{1.862}$, at High Temperature and in an Applied Electrical Field

BY HIROYUKI HORIUCHI,* ARTHUR J. SCHULTZ, PETER C. W. LEUNG AND JACK M. WILLIAMS

Chemistry and Materials Science and Technology Divisions, Argonne National Laboratory, Argonne, Illinois 60439, USA

(*Received* 10 *February* 1984; *accepted* 16 *April* 1984)

Abstract

Single-crystal time-of-flight neutron diffraction techniques have been applied to the analysis of oxygen behavior in the structure of yttria-stabilized cubic zirconia, $Zr(Y)O_{1.862}$. Reflection data were collected at room temperature, at 1040 K, and at 1040 K with a 7·8 DC voltage across the (100) and ($\bar{1}$00) crystal faces, which generated a 9–10 mA ionic current. On the difference Fourier maps derived from high-temperature data, residual peaks due to interstitial mobile oxygen ions were observed along ⟨100⟩ under the condition of an applied DC voltage. Residual peaks attributed to large anharmonic thermal vibrations along ⟨111⟩ were also observed.

Introduction

Single crystal time-of-flight (TOF) neutron diffraction is a particularly powerful technique for the study of crystal structures under special environmental conditions. In this paper we report on the application of this technique to the study of oxygen motion in yttria-stabilized cubic zirconia at high temperatures.

Yttria-stabilized zirconia (YSZ), in which the cation is partially substituted by Y, crystallizes in a cubic structure (fluorite type) at high temperatures. This cubic structure is oxygen deficient owing to the statistical substitution of ZrO_2 by Y_2O_3 and is stable over a wide temperature range. This material is a very good O^{2-}-ion conductor at temperatures exceeding 900 K. In order to elucidate the O-atom motion in the structure, YSZ has been studied extensively using X-ray and neutron diffraction techniques (Steel & Fender, 1974; Faber, Mueller & Cooper, 1978; Morinaga, Cohen & Faber, 1979). However, most of these studies have been made on products quenched from high temperatures.

Neutron diffraction is more advantageous than X-ray diffraction for determining the oxygen behavior in these structures because the ratio of the scattering amplitude of O to Zr and Y is much larger (1 : 1·22 : 1·36) and the absorption due to Zr and Y is much less for neutrons. Furthermore, the TOF technique combined with a position-sensitive area detector (Schultz, Srinivasan, Teller, Williams & Lukehart, 1984) minimizes the motion of the specimen and permits the collection of diffracted intensities with the simultaneous measurement of ionic conductivities at high temperatures.

In this work, we investigated the crystal structures of yttria-stabilized cubic zirconia at room temperature, at 1040 K, and at 1040 K with a 7·8 DC voltage applied across the (100) and ($\bar{1}$00) crystal faces,which generated ~9–10 mA ionic current. The single crystal used in this study has the chemical composition $0{\cdot}84ZrO_2.0{\cdot}16Y_2O_3$. Data were measured using the TOF single-crystal diffractometer

* Present address: Institute of Scientific and Industrial Research, Osaka University, 8–1 Mihogaoka, Ibaraki, Osaka 567, Japan.

0108-7681/84/040367-06$01.50

equipped with a unique, position-sensitive ^{6}Li-glass scintillation detector (Brenner, Chou, Strauss & Winiecki, 1982; Schultz, Teller, Williams, Strauss & Brenner, 1982) with an active area of 30×30 cm and a spatial resolution of 3·5 mm.

Direct measurements of ionic conductivities at various temperatures using two electrodes have also been made in order to characterize further the single-crystal specimens.

Experiments

Specimen

A completely colorless and transparent single-crystal specimen was used for this experiment (supplied from Nakazumi Earth Crystal Ltd, Osaka, Japan). The crystal was grown by the cold crucible method. Observations made with polarized light indicated the specimen was optically isotropic, and therefore the crystal system was assumed to be cubic. X-ray diffraction precession photographs exhibited *F*-centered cubic symmetry, and therefore the space group was assumed to be $Fm3m$, which is the same as that of the fluorite structure.

The chemical composition was analyzed by means of an analytical electron microscope equipped with an Si(Li) solid-state detector (Hitachi-12SE, Institute of Scientific and Industrial Research, Osaka University, Japan) over the energy range from about 1 to 40 keV ($1\text{ eV} = 1{\cdot}6\times10^{-19}$ J). Only characteristic X-ray spectra corresponding to Cu($K\alpha$ and $K\beta$), Zr($L\alpha$, $K\alpha$ and $K\beta$) and Y($K\alpha$ and $K\beta$) were observed. The observed spectra for Cu were due to the specimen holder. Quantitative analysis of the integrated intensities yielded the atomic ratio $Y/(Zr+Y) = 0{\cdot}28(2)$, which gives a chemical stoichiometry of $0{\cdot}84ZrO_2 . 0{\cdot}16Y_2O_3$ or $Zr(Y)O_{1.862}$, assuming an oxygen-deficient structure.

The density of 5·845 g cm^{-3}, measured pycnometrically at room temperature, is in good agreement with the calculated density of 5·824 g cm^{-3} for the oxygen-deficient structure using a lattice constant of $a = 5{\cdot}158$ Å. The lattice parameters were determined from a spherically shaped single crystal using a four-circle X-ray diffractometer.

A few cubic-shaped specimens bounded by {100} faces, with edges of 3 mm, were cut from a large as-grown crystal and were used for the O^{2-} ionic conductivity measurements and for the neutron diffraction studies.

O^{2-} *ionic conductivity*

O^{2-} ionic conductivities were measured across the (100) and ($\bar{1}00$) planes between room temperature and 1270 K. Platinum grids were used as electrodes and were fixed to the crystal specimen using a platinum paste at 1370 K for 10 min. Typical plots of ionic conductivity *versus* inverse temperature are shown in Fig. 1. The rate of temperature increase is about 3 K min^{-1}. The magnitudes of the conductivities vary for each experiment, especially at lower temperature, and the conductivity *versus* temperature curves are different for the cases of increasing and decreasing temperatures. Similar observations have been reported by Kobayashi (1981). The relatively high conductivity at low temperature in experiments in which the temperature is increasing is apparently due to extrinsic factors such as rearrangements of frozen defects and/or interstitial atoms. The conductivity above about 900 K is assumed to be due mainly to the intrinsic oxygen-ion current in the structure. Therefore, the thermal history applied to the specimen, and the gradient of increasing or decreasing temperature will also affect the values of conductivity as well as the defect structure, especially at low temperatures. More detailed experimental results and discussions on single-crystal ionic conductivity will be reported elsewhere.

Neutron diffraction with the TOF technique

Neutron diffraction experiments were made under the following three conditions: (1) at room temperature, (2) at 1040 K, and (3) at 1040 K with a 7·8 DC voltage applied across the (100) and ($\bar{1}00$) faces of the crystal, which produced an ionic current of ~9–10 mA across the two faces of the specimen. In each histogram, a neutron TOF range of 1·2 to 6·2 ms, corresponding to a wavelength range of 0·7 to 3·6 Å, was used. The TOF histogram intervals

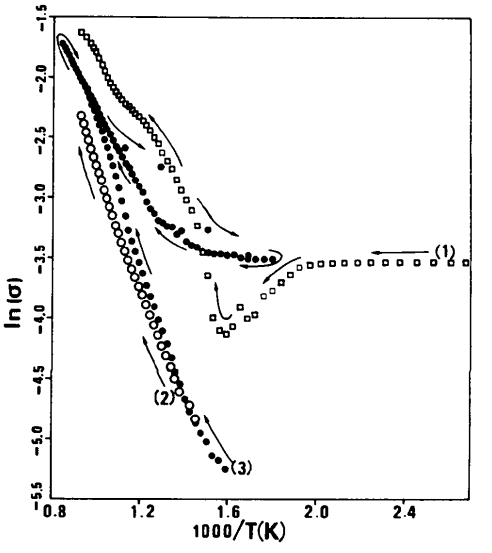

Fig. 1. Ionic conductivity, ln(σ), *versus* inverse temperature. Three independent runs are shown: (1) 6 volts, temperature increasing from room temperature to 1078 K; (2) 3 volts, temperature increasing from room temperature to 1078 K; (3) 6 volts, temperature increasing from room temperature to 1078 K, then decreasing to 556 K, and again increasing to 1064 K.

Table 1. *Instrument and data-collection parameters*

Sample-to-detector distance	28·0 cm
Sample-to-moderator distance	661·44 cm
Detector angle	90·00°
ω angle	45·00°
Effective detector dimensions	27·6 × 27·2 cm
Neutron source repetition rate	30 pulses s^{-1}
Histogram dimensions ($X \times Y \times T$)	85 × 85 × 112 channels
Wavelength range	0·70 – 3·60 Å
Detector channel widths ($\Delta X \times \Delta Y$)	0·32 × 0·32 cm
Time channel width (Δt)	45 μs (0·026 Å)

were 45 μs (0·026 Å), which resulted in 112 time channels along the wavelength axis. Thirteen histograms covering one octant of reciprocal space were obtained using appropriate combinations of χ and φ angles of the four-circle diffractometer. The detector and ω angles were fixed at 90 and 45°, respectively. The crystal and detector remain stationary while data are being collected. Instrument parameters such as sample-to-detector distance, the center position of the area detector and the effective detector dimensions were determined using an NaCl single crystal (Schultz, Teller, Williams, Strauss & Brenner, 1982). A summary of the instrument and data-collection parameters is presented in Table 1.

Data collection at high temperatures

A high-temperature furnace was designed and constructed to collect high-temperature data on a single crystal (Fig. 2). The furnace is stationary during data collection and is suspended in the center of the diffractometer with openings in the outer alumina container for the incident and unscattered beam and for the neutrons scattered by the crystal toward the detector. A crystal specimen was mounted on a silica-glass rod which was inserted through a slit in the furnace, which permitted the crystal to be rotated more than 90° in χ and a full 360° in φ. A cylindrical platinum foil with a thickness of 30 μm was used as a heating element, which permitted temperatures of over 1000 K to be achieved. The space between the platinum foil and alumina cylinder was filled with quartz-glass wool to provide thermal insulation and keep a uniform temperature around the specimen. The temperature was controlled within a fluctuation of ±5 K at around 1000 K.

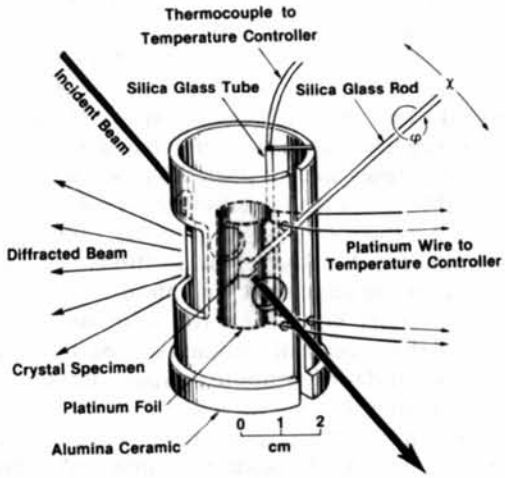

Fig. 2. Perspective view of the furnace designed for this experiment.

Data analysis

High backgrounds due to scattering by the furnace materials were observed in the high-temperature experiments. These background intensities were successfully eliminated by subtracting a background histogram obtained with only the furnace (without specimen) in position from each of the histograms collected with both the specimen and the furnace mounted on the diffractometer. Plots of one Laue histogram are shown in Figs. 3(*a*) and 3(*b*).

After subtraction of backgrounds, reflections in each histogram were located using a three-dimensional peak-search routine and the results were stored in a file with appropriate positional and wavelength information. Several Bragg peaks were first indexed using lattice constants determined by X-ray diffraction ($a = 5{\cdot}158$ Å) and a preliminary orientation matrix was obtained and was used to index the remaining peaks. Precise lattice parameters

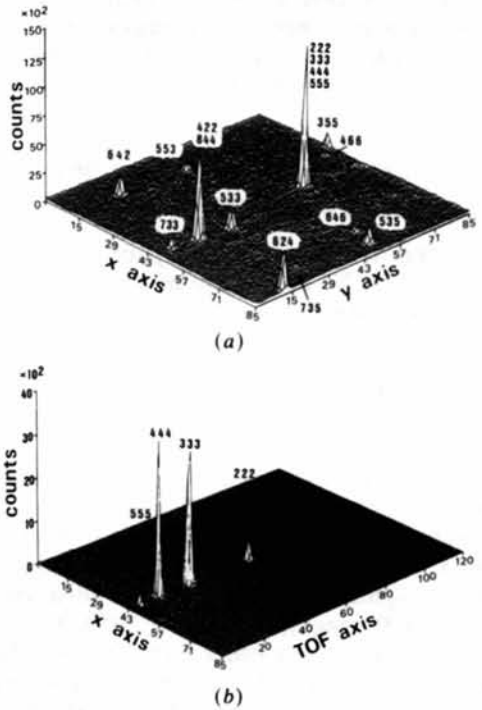

(*a*)

(*b*)

Fig. 3. A histogram obtained at 1040 K and 7·8 DC volts across the crystal. (*a*) The Laue pattern showing a projection for all 112 time channels ($\lambda = 0{\cdot}70 - 3{\cdot}60$ Å). The x and y channel numbers represent vertical and horizontal position, respectively, on the detector. (*b*) *hhh* reflections on the x–t section of the histogram at $y = 63$ [see (*a*)].

and an orientation matrix were determined by a least-squares fit of the observed peak positions. This same procedure was followed in each of the three experiments. The lattice constants are 5·17(2), 5·21(2) and 5·21(2) Å for experiments (1), (2) and (3), respectively.

The intensity of each possible Bragg reflection was obtained by integrating a three-dimensional region around the histogram peak location calculated from the orientation matrix. The relationship between integrated intensity, $I(hkl)$, and structure factor amplitude, $F(hkl)$, is:

$$I(hkl) = kT.\varphi(\lambda).\varepsilon(\lambda).A(\lambda).y(\lambda) \times |F(hkl)|^2\lambda^4/\sin^2\theta, \quad (1)$$

where k is a scale factor, T is the factor to normalize all histograms based on monitor counts, λ is the wavelength and θ is the Bragg angle. The wavelength-dependent factors for the incident flux $\varphi(\lambda)$ and the detector efficiency $\varepsilon(\lambda)$ were obtained from the incoherent scattering from a vanadium sample. The absorption coefficients for the crystal at $\lambda = 0{\cdot}7$ Å ($\mu = 0{\cdot}350\ cm^{-1}$) and at $\lambda = 3{\cdot}6$ Å ($\mu = 0{\cdot}394\ cm^{-1}$) were used to calculate the absorption-correction factors $A(\lambda)$ for the $3\times3\times3$ mm cube specimen. Extinction-correction factors $y(\lambda)$ were obtained by least-squares fitting between observed and calculated structure factors. A review of the single-crystal TOF neutron diffraction technique using an area detector and its application to single-crystal structure analysis have been reported (Schultz *et al.*, 1984).

Structure analysis and discussion

Structure analysis and results

In the fluorite-type structure (space group $Fm3m$) the cations (Zr, Y) and O atoms are located at the following positions:

cations:	4(*a*)	*m*3*m*	0,	0,	0	+ (000, $\frac{1}{2}\frac{1}{2}$0, $\frac{1}{2}$0$\frac{1}{2}$, 0$\frac{1}{2}\frac{1}{2}$).
O atoms:	8(*c*)	$\bar{4}3m$	$\frac{1}{4}$,	$\frac{1}{4}$,	$\frac{1}{4}$	
			$\frac{3}{4}$,	$\frac{3}{4}$,	$\frac{3}{4}$	

The cation sites were assumed to be statistically occupied by Zr and Y atoms. From a neutron diffraction analysis of a sample quenched from about 1670 K, Carter & Roth (1968) suggested that the O atoms are slightly displaced from the ideal position of ($\frac{1}{4}$, $\frac{1}{4}$, $\frac{1}{4}$), with magnitudes of ~0·2–0·3 Å along the ⟨111⟩ direction. On the other hand, Steel & Fender (1974) reported that in the structures of $Zr(Y)O_{1.87}$ and $Zr(Yb)O_{1.87}$ a large proportion of the O atoms are displaced along the ⟨100⟩ direction by about 0·4 Å, and a small proportion are displaced along ⟨111⟩ by about 0·5 Å, based on neutron powder diffraction data. Morinaga, Cohen & Faber (1979) studied the structures of $Zr(Y)O_{1.893}$ and $Zr(Ca)O_{1.866}$ using single-crystal X-ray diffraction and reported that the O atoms of $Zr(Y)O_{1.893}$ show displacements similar to those reported by Steel & Fender for $Zr(Y)O_{1.87}$, with amplitudes of 0·26 and 0·13 Å along ⟨100⟩ and ⟨111⟩, respectively. However, in $Zr(Ca)O_{1.866}$ the shifts are along the ⟨100⟩ direction. Thus the O-atom positions, which provide an important key to understanding the oxygen motion at high temperatures, are still ambiguous. The most likely displacements of O atoms are summarized as follows:

8(*c*)	$\bar{4}3m$	→ 8(*c*)	$\bar{4}3m$	no displacement
		→ 32(*f*)	3*m*	($\frac{1}{4}+\delta, \frac{1}{4}+\delta, \frac{1}{4}+\delta$)
		→ 48(*g*)	*mm*	($\frac{1}{4}+\delta, \frac{1}{4}, \frac{1}{4}$).

In this structure analysis, most of the data analyses were accomplished with a library of programs residing on a VAX 11/780 computer at the Intense Pulsed Neutron Source of Argonne National Laboratory. As a first step, the least-squares fitting between observed and calculated intensities was carried out with four variables consisting of one overall scale factor, an isotropic-extinction parameter and individual isotropic temperature factors for the cation and anion atoms. Relatively larger temperature factors were observed for O atoms than for the cations for both the room- and high-temperature structures, and their magnitudes increased at high temperatures.

The difference Fourier synthesis $\rho_{obs}(r) - \rho_{calc}(r)$, where $\rho_{calc}(r)$ is the calculated density using regular positions for cation and O atoms and individual isotropic temperature factors, showed a displacement of O atoms from their ideal positions [see Fig. 4(I)(*a*), (*b*) and (*c*)], especially in the ⟨111⟩ direction in the high-temperature structures. We consider that these spatial displacements are mainly due to anharmonic thermal vibrations because these factors are strongly correlated to the temperature increase. The displacements along ⟨100⟩ are also observed, especially in the high-temperature and applied-DC-voltage structure. In the difference Fourier maps in Fig. 4(I)(*c*), the residual peaks at $x = 0{\cdot}20$ and $x = \frac{1}{4}$ indicate displacements along ⟨111⟩ and ⟨100⟩, respectively.

As a second step, in order to evaluate the magnitudes and directions of the thermal vibrations of the O atoms, the least-squares refinements and difference Fourier syntheses were repeated by placing O atoms at the slightly displaced positions of ($\frac{1}{4}+\delta, \frac{1}{4}+\delta, \frac{1}{4}+\delta$) along ⟨111⟩ and/or ($\frac{1}{4}+\delta, \frac{1}{4}, \frac{1}{4}$) along ⟨100⟩, and in their symmetrically equivalent positions. This statistical spatial arrangement of atoms, a so-called split-atom model, is sufficient for estimating the magnitudes of the spread of atomic distributions due to anharmonic and/or harmonic thermal vibrations as a first approximation.

Refinements of the displacement δ and occupancy number of the 32(*f*) position combined with the occupancy number of the 8(*c*) position were carried

out. This resulted in a small but negative occupancy value for the 8(*c*) position for all three sets of experimental data. Therefore, in the case of the refinement of the occupancy number of the 32(*f*) position, the occupancy of the 8(*c*) position was considered to be zero. That is, all of the O atoms were slightly shifted along the ⟨111⟩ direction. These results show that the magnitude of the displacement δ along ⟨111⟩ is larger at high temperature than at room temperature.

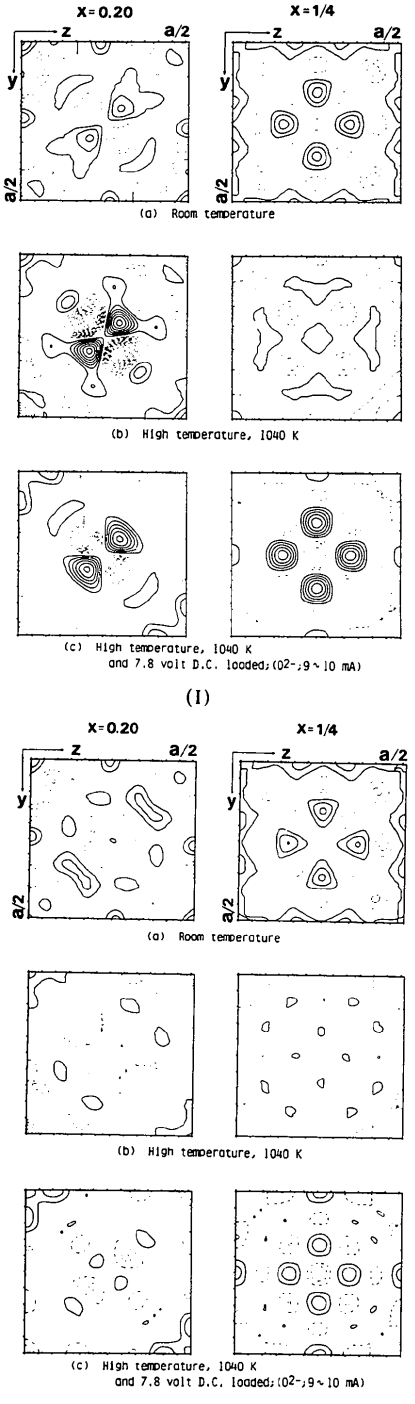

Fig. 4. (I) Difference Fourier maps, $\rho_{obs}(r)-\rho_{calc}(r)$, where $\rho_{calc}(r)$ is calculated density with ideal O position $(\frac{1}{4}, \frac{1}{4}, \frac{1}{4})$. (II) Difference Fourier maps, $\rho_{obs}(r)-\rho_{calc}(r)$, where $\rho_{calc}(r)$ is based on the final results of the split-atom mode for O atoms.

Table 2. *Results of refinements*

	Room temperature	1040 K	1040 K and 7·8 DC volts 9–10 mA ionic currents
Reflections used	140	133	128
Independent reflections	38	38	37
Oxygen: position 8(*c*)			
Fixed at $(\frac{1}{4}, \frac{1}{4}, \frac{1}{4})$			
$B(M)$(Å^2)	0·63 (9)	1·0 (1)	1·7 (2)
B(Ox)(Å^2)	1·9 (1)	2·6 (1)	2·2 (2)
$R(F)$	0·073	0·096	0·088
$wR(I)$	0·143	0·154	0·150
Oxygen: 8(*c*) → 32(*f*)			
Displaced to $(\frac{1}{4}+\delta, \frac{1}{4}+\delta, \frac{1}{4}+\delta)$			
$B(M)$(Å^2)	0·62 (9)	1·0 (1)	1·2 (2)
B(Ox)(Å^2)	1·2 (2)	1·4 (2)	1·0 (2)
δ	0·018 (2) (0·16 Å)	0·021 (1) (0·19 Å)	0·022 (1) (0·20 Å)
$R(F)$	0·073	0·091	0·079
$wR(I)$	0·142	0·145	0·138
Oxygen: 8(*c*) → 32(*f*) and 48(*g*)			
Displaced to $(\frac{1}{4}+\delta, \frac{1}{4}+\delta, \frac{1}{4}+\delta)$ and to $(\frac{1}{4}+\delta, \frac{1}{4}, \frac{1}{4})$			
$B(M)$(Å^2)		1·2 (1)	1·1 (1)
B(Ox)(Å^2)		1·3 (2)	1·0 (2)
δ[32(*f*)]		0·022 (1) (0·20 Å)	0·022 (1) (0·20 Å)
δ[48(*g*)]		0·14 (2) (0·73 Å)	0·12 (2) (0·62 Å)
Ratio of Ox[48(*g*)]/total (Ox)		0·07 (3)	0·11 (4)
$R(F)$		0·079	0·072
$wR(I)$		0·136	0·130

Refinements of the displacement and occupancy value of the 48(*g*) position were carried out next in combination with the occupancy and δ value of the 32(*f*) position. In the two high-temperature structures, we find a portion of the O atoms are displaced along ⟨100⟩. In particular, the structure with the O^{2-} ionic current due to the applied DC voltage shows displacements of a larger percentage of the O atoms than in the other structures. Furthermore, in the refinement of the room-temperature structure we did not find any significant proportion of O atoms displaced along ⟨100⟩. We also found no improvement in the R factor for the trial structure in which we placed O atoms at the $(\frac{1}{4}+\delta, \frac{1}{4}, \frac{1}{4})$ positions, although we did observe some small peaks along ⟨100⟩ on the difference Fourier map [Fig. 4(I)(*a*)].

The results of the refinements are summarized in Table 2.* The residual peaks on the difference Fourier maps around the O positions [Fig. 4(II)(*a*), (*b*) and (*c*)], which were calculated based on the final atomic parameters including split-atom positions, are much smaller than those shown in Fig. 4(I)(*a*), (*b*) and (*c*).

* Lists of structure factors have been deposited with the British Library Lending Division as Supplementary Publication No. SUP 39397 (5pp.). Copies may be obtained through The Executive Secretary, International Union of Crystallography, 5 Abbey Square, Chester CH1 2HU, England.

This result demonstrates that the split-atom model is sufficient for accounting for atom displacements due to anharmonic and/or harmonic thermal vibrations and/or interstitial atoms accompanied by mobile O atoms.

Discussion

The main sources of the observed displacements of the O atoms from their ideal positions are (1) statistical spatial distributions of Y_2O_3 moieties which are essentially fluorite type but which also include oxygen defects, (2) anharmonic and/or harmonic thermal vibrations at high temperature, and (3) mobile and/or hopping O^{2-} ions at high temperature through vacant positions, especially under an applied DC voltage.

A schematic illustration of O-atom displacements in the structure of Y_2O_3 is illustrated in Fig. 5 (Paton & Maslen, 1965; Bonnet, Delapalme & Fuess, 1975). The directions of the displacements are shown by arrows. These displacements are not only in the (001) plane but also directed above and below the plane. The magnitude of the deviation is about 0·35 Å from the ideal position. In the ideal fluorite-type structure, vacancies are all filled by O atoms and there are no displacements. Therefore, the observed displacements along ⟨111⟩ at room temperature are the average displacements which are mainly attributed to statistical arrangement of Y_2O_3-type clusters in the structure.

In the room-temperature structure, it might have been appropriate to fix some atoms on interstitial sites along ⟨111⟩ and/or ⟨100⟩, depending on the particular heat treatment in the sample preparation. However, the residual peak height on the difference Fourier map was quite low in this experiment, and this result indicates that the relative amount of interstitial atoms is quite small at room temperature.

In high-temperature structures, strong anharmonic thermal vibrations were observed along ⟨111⟩ as shown in Fig. 4(I)(*b*) and (*c*). Residual peaks along ⟨100⟩ were only clearly observed in the case in which DC voltage was applied across the (100) and ($\bar{1}$00) crystal faces. Therefore, it is expected that an ionic current occurs with mobile O^{2-} ions moving along ⟨100⟩ through vacant O sites.

Since DC voltage was applied across the (100) and ($\bar{1}$00) faces, we might expect some anisotropic diffusion of O^{2-} ions in the crystal which would affect the symmetry of the structure. For the data we collected there were no significant differences of intensities among equivalent reflections of Laue group $m3m$ within the experimental errors. Therefore, in this structure analysis the symmetry was assumed to be $Fm3m$. However, it is possible that at higher temperatures with a higher ionic current, a high-resolution data collection could exhibit some anisotropy, such as peak broadening or diffuse scattering, due to the motion of mobile O^{2-} ions. In fact, the 10 mA ionic current of this experiment only corresponds to about 35 ions $Å^{-2}\,s^{-1}$, which may not be sufficient to produce observable anisotropic scattering. Furthermore, random motion obeying cubic symmetry may be dominant in the crystal structure even in the applied-DC-voltage condition.

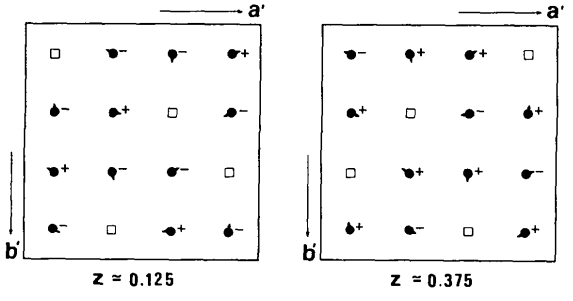

Fig. 5. Oxygen arrangements and their direction of displacements in the structure of Y_2O_3, where $a' = b' = c' = 10{\cdot}604$ Å. The open squares represent the O vacant sites, and the arrows indicate the direction of the component of the displacement in the plane and + or − represents the component of the vector above or below the plane, respectively. The relationship between the a of YSZ and a' is $a = a'/2$.

HH greatly appreciates the financial support from the Intense Pulsed Neutron Source and the Chemistry and Materials Science and Technology Divisions of Argonne National Laboratory, USA, for the opportunity to carry out this experiment. We wish to thank Dr Toshio Maruyama, Tokyo Institute of Technology, Japan, for his helpful suggestions on the ionic-conductivity measurements of yttria-stabilized cubic zirconia, and Dr Mark Beno, Argonne National Laboratory, for his technical help on computer operations and on high-temperature experiments. We also wish to acknowledge the support of the Office of Basic Energy Science, Division of Materials Science, US Department of Energy, under contract W-31-109-Eng-38.

References

BONNET, M., DELAPALME, A. & FUESS, H. (1975). *Acta Cryst.* A**31**, 264–265.

BRENNER, R., CHOU, H. P., STRAUSS, M. G. & WINIECKI, A. L. (1982). *IEEE Trans. Nucl. Sci.* **29**, 207–211.

CARTER, R. E. & ROTH, W. L. (1968). *EMF Measurement in High Temperature Systems*, edited by C. B. Alcock, pp. 125–144. New York: The Institute of Mining and Metallurgy.

FABER, J. JR, MUELLER, M. H. & COOPER, B. R. (1978). *Phys. Rev. B*, **17**, 4884–4888.

KOBAYASHI, S. (1981). *Yogyo-Kyokai-Shi*, **88**, 14–22.

MORINAGA, M., COHEN, J. B. & FABER, J. JR (1979). *Acta Cryst.* A**35**, 789–795.

PATON, M. G. & MASLEN, E. N. (1965). *Acta Cryst.* **19**, 307–310.

SCHULTZ, A. J., SRINIVASAN, K., TELLER, R. G., WILLIAMS, J. M. & LUKEHART, C. M. (1984). *J. Am. Chem. Soc.* **106**. In the press.

SCHULTZ, A. J., TELLER, R. G., WILLIAMS, J. M., STRAUSS, M. G. & BRENNER, R. (1982). *Trans. Am. Crystallogr. Assoc.* **18** 169–179.

STEEL, D. & FENDER, B. E. F. (1974). *J. Phys. C*, **7**, 1–11.